

Underactuated Control of Multiple Soft Pneumatic Actuators via Stable Inversion

Wu-Te Yang¹, *IEEE Student Member*, Burak Kurkcu², *IEEE Member*,
Masayoshi Tomizuka¹, *IEEE Life Fellow*

Abstract—Soft grippers, with their inherent compliance and adaptability, show advantages for delicate and versatile manipulation tasks in robotics. This paper presents a novel approach to underactuated control of multiple soft actuators, specifically focusing on the synchronization of soft fingers within a soft gripper. Utilizing a single syringe pump as the actuation mechanism, we address the challenge of coordinating multiple degrees of freedom of a compliant system. The theoretical framework applies concepts from stable inversion theory, adapting them to the unique dynamics of the underactuated soft gripper. Through meticulous mechatronic system design and controller synthesis, we demonstrate both in simulation and experimentation the efficacy and applicability of our approach in achieving precise and synchronized manipulation tasks. Our findings not only contribute to the advancement of soft robot control but also offer practical insights into the design and control of underactuated systems for real-world applications.

Index Terms—Underactuated control, algebraic control, soft actuator, soft robot, system perturbation.

I. INTRODUCTION

SOFT robotics has become an emerging field, offering solutions for tasks that traditional robots struggle to accomplish. In particular, the inherent compliance and adaptability of soft actuators show advantages for applications requiring delicate manipulation [1], [2] and interaction with complex or unknown environments [3], [4]. Compared to rigid-bodied robotic hands, soft grippers stand out for their ability to conform to a wide range of object shapes and sizes, making them indispensable in domains such as medical robots [5] and human-robot interactions [6]. However, achieving precise control over the motion and coordination of multiple soft fingers within a gripper remains a challenge [7]. The particularly evident issue is underactuated control, where the number of actuators exceeds the number of control inputs, leading to restricted motions. Moreover, the air pump occupies space and has a certain weight, so reducing the number of inputs saves space and reduces weight and costs [8]. In this context, the development of effective underactuated control strategies tailored to the characteristics of soft robotics is essential to unlock their potential in real-world applications.

Despite the recent development of soft robot control, achieving precise control under the underactuated control framework for soft robots is seldom discussed and remains a challenge.

¹The authors are with the Department of Mechanical Engineering, University of California, Berkeley, MSC Lab, USA wtyang; tomizuka@berkeley.edu

²The author is a Research Scholar at the University of California, Berkeley, USA bkurkcu@berkeley.edu

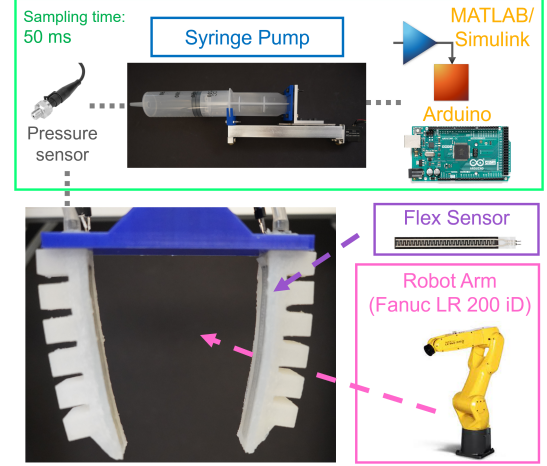


Fig. 1. The soft gripper has two fingers and is driven by a single syringe pump to achieve underactuated control via algebraic approaches. The control commands are generated in MATLAB/Simulink and are converted to PWM for the stepper motor in the syringe pump. The bending angles of both fingers are measured by the flex sensor embedded in each soft gripper.

A couple of works addressed the soft robot control issues by applying nonlinear controllers [9], [10], adaptive controllers [11], [12], and optimal controllers [7], [13]. Those control strategies enable high-performance control of soft robots with high degrees of freedom. However, the control of these systems becomes increasingly complex as the number of degrees of outputs exceeds that of inputs (underactuated control). Furthermore, soft materials have an uncertain nature and thus soft robots exhibit model uncertainty. When they work in unstructured environments, the robustness of the controller becomes more important. Addressing this challenge may require the development of novel control strategies that can effectively synchronize multiple soft actuators within a soft gripper, enabling precise and adaptive manipulation tasks in real-world scenarios.

The primary objective of this paper is to develop control algorithms for achieving synchronization in multi-finger soft grippers. These mechatronic systems are designed and modeled to establish a non-square system matrix for single-input-multiple-output (SIMO) control scenarios. Our approach integrates both feedforward and feedback control loops. The feedforward control mechanism incorporates a stable model inversion technique that effectively synchronizes the motions of multiple soft fingers. Given the inherent uncertainty of soft materials, the feedback loop is adept at mitigating un-

expected errors, noise, or disturbances that may arise between the mathematical model and the real system. Comprehensive validation of the control algorithms is conducted through simulations and experimentation. The theoretical framework underpinning these control algorithms is initially introduced in [14], where its efficacy is established by necessary and sufficient conditions. The contributions of this research lie in the innovative application of stable inversion control algorithms to address uncertain soft robotic systems. Notably, the proposed controller achieves synchronization of multi-finger soft grippers with a single input, thereby demonstrating the applicability of these control algorithms to SIMO control problems.

To position our contributions, we compare our research with recent works. In our prior study [7], we employed individual optimal controllers for each finger within a multi-finger soft gripper (fully actuated) to attain precise and synchronized motions. In contrast, the present research adopts algebraic control algorithms alongside a single air pump to achieve synchronization across all fingers within the multi-finger soft gripper. Keppler et al. [15] established input coordination transformation that made the underactuated soft robotic systems become quasi-fully actuated systems. Although our feed-forward control uses a similar concept, there is a feedback loop to cope with the uncertainty of the soft robotic systems that ensures robustness of the system. Pustina et al. [16] studied the controllability and stability of the underactuated soft robots. But our work focuses on the SIMO problem of synchronizing motions of multiple soft robots with a single input. Overall, this research studies the stable underactuation and synchronization of soft robots with robustness performance.

The remainder of this paper is organized as follows. Section II introduces the mathematics preliminary and problem statement. Section III describes the full mechatronic design and algebraic controller design. Section IV evaluates the feasibility and applicability of the controller by simulations and experimentation. Section V discusses the experimental results and concludes the work.

II. PROBLEM FORMULATION

A. Mathematics Preliminaries

The set \mathbb{R} is a field of real number. Then, the set of polynomials in s with coefficients from \mathbb{R} is denoted as $R(s)$. This set is a structured domain, a commutative ring over \mathbb{R} , labeled as $\mathbb{R}[s]$. The set, say \mathcal{R} , is an *integral domain* if this ring has an identity element and no zero divisors. A Euclidean Domain, labeled as D , is an integral domain paired with a Euclidean function denoted as $f : D \setminus \{0\} \rightarrow \mathbb{N}$, where \mathbb{N} represents the set of integer numbers. To simplify, for any two elements a and $b \in D$ where b is not equal to 0, there are two other elements q and r in D such that $a = bq + r$, where r can be 0 or the value of $f(r) < f(b)$.

Given that $n(s), d(s) \in R[s]$ and $d(s) \neq 0$, the equation $n(s)/d(s)$ exists. The set of all these rational functions in s over R forms a field, denoted by $R(s)$ [17], and it holds that $R[s] \subset R(s)$. The sets of $n_y \times n_u$ matrices with elements in $R, R[s]$, and $R(s)$ are denoted by $R^{n_y \times n_u}, R[s]^{n_y \times n_u},$

and $R(s)^{n_y \times n_u}$ respectively. The $R[s]$ is an Euclidean domain [14], [18]. In this paper, the order of a polynomial basis is defined as the degrees of its vectors.

Theorem 1. (Rouche-Capelli Theorem) Let $P \in \mathbb{R}(s)^{n_y \times n_u}$ be a matrix and $y \in \mathbb{R}(s)^{n_y \times 1}$ be a vector. If $\text{rank}(P) = \text{rank}([P \mid y])$, which is necessary and sufficient for $Pu = y$ to have a solution, the following statements hold:

- C1. If $\text{rank}(P) = n_u \leq n_y$, the system has a unique solution.
- C2. If $\text{rank}(P) = n_y < n_u$, the system has infinitely many solutions with $n_u - n_y$ free variables.
- C3. If $\text{rank}(P) < \min(n_y, n_u)$, the system has infinitely many solutions with $n_u - \text{rank}(P)$ free variables.

The definition in [19] is referenced to clarify the notation. The rank of a matrix over the field $\mathbb{R}(s)$ is defined as the maximum number of linearly independent subsets of its columns (or rows) with respect to $\mathbb{R}(s)$. This is denoted by $\text{rank}_{\mathbb{R}(s)}(P)$. If a set of vectors v_1, v_2, \dots, v_{n_u} is linearly independent in the field $\mathbb{R}(s)$ if and only if the condition $\sum a_i v_i = 0$ and $a_i = 0$ for every i with the scalars a_i in $\mathbb{R}(s)$.

Suppose the rank of $P(s) \in \mathbb{R}(s)^{n_y \times n_u}$ is r and $1 \leq r \leq \min(n_u, n_y)$. Let the columns of $P(s) = [p_1, p_2, \dots, p_{n_u}]$. Then, $\mathcal{L}(P)$ represents the set of r linearly independent columns of $P(s)$ and defined as

$$\mathcal{L}(P) = \{p_i \in P(s) : 1 \leq i \leq r\} \quad (1)$$

with p_i being linearly independent over $\mathbb{R}(s)$. We next introduce the subspace of $\mathbb{R}(s)^{n_y}$ spanned by these linearly independent columns

$$\text{Im}_{\mathbb{R}(s)}(P) = \left\{ \sum_{i=1}^r c_i p_i : c_i \in \mathbb{R}(s), p_i \in \mathcal{L}(P) \right\} \subset \mathbb{R}(s)^{n_y} \quad (2)$$

The null space of $P(s)$ in the field $\mathbb{R}(s)$ is denoted as $\text{Ker}_{\mathbb{R}(s)}(P)$. Let $\mathbb{R}[s]_- = \{n(s) \in \mathbb{R}[s] : \Re(\rho) < 0, \forall \rho \text{ s.t. } n(\rho) = 0\}$ denote the set of polynomials in $\mathbb{R}[s]$ whose roots all have negative real parts and $\mathbb{R}(s)_- = \{n(s)/d(s) \in \mathbb{R}(s) : d(s) \in \mathbb{R}[s]_-\}$ represents the set of rational functions in $\mathbb{R}(s)$ whose denominators belong to \mathbb{R}_- . The $\Re(\cdot)$ represents the real part of the given complex number and $\Im(\cdot)$ denotes the imaginary part of the number.

B. Problem Statement

The soft gripper is used as the plant for the proposed control algorithms. Although soft robots inherently possess nonlinear characteristics [20], the nonlinearity is often not obvious under restricted deformations. Thus, within the confines of limited deformations, soft robots can be effectively approximated using linear models. Consequently, the system can be described using a standard state-space representation [21].

Consider the multi-input-multi-output (MIMO) linear time-invariant (LTI) system

$$\begin{aligned} \dot{x} &= Ax + Bu \\ y &= Cx, x(0) = 0 \end{aligned} \quad (3)$$

where $A \in \mathbb{R}^{n \times n}$, $B \in \mathbb{R}^{n \times n_u}$, $C \in \mathbb{R}^{n_y \times n}$, $x(t)$ and $x_0 \in \mathbb{R}^{n \times 1}$, $y(t) \in \mathbb{R}^{n_y \times 1}$, and $u(t) \in \mathbb{R}^{n_u \times 1}$. It is assumed that the (4) is Hurwitz and minimum phase system.

Assumption 1. *The system given in (3) is minimal or is transformed into minimal realization.*

The (3) can be solved mathematically and the derived equation in the Laplace domain ($\mathcal{L}\{f(t)\} = F(s)$ [22]) is shown below

$$\begin{aligned} Y(s) &= C(s)(sI - A)^{-1}BU(s) \\ \Rightarrow Y(s) &= P(s)U(s) \end{aligned} \quad (4)$$

The (4) can be expressed as

$$\begin{bmatrix} Y_1(s) \\ \vdots \\ Y_n(s) \end{bmatrix} = \begin{bmatrix} P_1(s) \\ \vdots \\ P_n(s) \end{bmatrix} U(s) \quad (5)$$

where $P_i(s) \in \mathbb{R}(s)^{n \times 1}$, $Y_i(s) \in \mathbb{R}(s)^{n \times 1}$, $i = 1 \dots n$, and $U(s) \in \mathbb{R}(s)$ so all elements in $P(s)$ and $Y(s)$ belongs to $\mathbb{R}(s)$. Also, the $Y(s)$ is in the range space of $P(s)$ and it is denoted as $Y(s) \in \text{Im}_{\mathbb{R}(s)}(P)$. The system equation (5) can be analyzed in an algebraic manner. According to the *Theorem 1*, the (5) exists a unique solution and the $U(s)$ can be obtained. Since the system is Hurwitz and minimum phase, the solution, model inversion of $P(s)$, is stable. Thus, the solution exists and is stable.

III. METHODOLOGY

In this section, we thoroughly introduce the mechatronic system design including the soft pneumatic actuators [21], [23] and syringe pump design [24]. The research delves into the study of a soft gripper system formed by integrating those components. The soft pneumatic actuators serve as the fingers driven by the syringe pump and the algebraic control algorithms. The dynamical modeling of the systems based on mechanics and fluid dynamics theories is disclosed in Sec. III-B. The algebraic controller is designed based on the dynamical model as introduced in Sec. III-C.

A. Mechatronic Design

The mechatronic system design can be illustrated in Fig. 2 (a), (b), and (c). The soft gripper is composed of two main components such as soft fingers and a syringe pump as in Fig. 1. The design methodology of each component will be elaborated in the following paragraphs.

1) *Soft Actuator Design:* The soft actuator is designed under an optimal model-based design framework which considers force/torque, bendability, and controllability simultaneously during the design stage [21]. The dimensional parameters of a soft pneumatic actuator is displayed in Fig. 2 (a), which is the cross-sectional view of the soft actuator's chamber room. The optimal dimensional parameters are searched by the optimization framework below

$$\begin{aligned} \max_{a,b,w,t} & \bar{T}(p) + \bar{\theta}(p) \\ \text{s.t. } & \dot{p} = 0 \\ & a_1 \leq a \leq a_2 \\ & b_1 \leq b \leq b_2 \\ & h_1 \leq a + b \leq h_2 \\ & C_1 \leq Ew(a + b)^{n+2} \leq C_2 \end{aligned} \quad (6)$$

where a is the top of the chamber to the neutral surface, b is the neutral surface to the bottom of the chamber, $a + b$ is the height of the soft actuator as in Fig. 2 (a), E is Young's modulus of the selected material, and n is a parameter related to soft materials and determined by experiments [25]. Note that w and t represent the width and wall thickness of the cross-sectional area (Fig. 2 (a)). However, they usually hit the upper and lower bounds respectively, so they are not included in the (6) and determined by the designer.

The $\bar{T}(p)$ represents the Pressure-to-Force/Torque model which is obtained by mechanics analysis of the soft actuator [21], while the $\bar{\theta}(p)$ stands for the Pressure-to-Bending model which is derived by a nonlinear mechanics theory [21], [25]. The constraint of $Ew(a + b)^n$ aims to place the natural frequency of the soft actuator in the desired range. The remaining parameters which are not considered in the (6) include the Young modulus, length of the structure, and number of chamber rooms. They will be discussed in the following paragraph.

The range of dimensional parameters is selected by referencing the size of human fingers [26], [27], so the constraint of a , b , and the value of w are determined and n is decided by the selected soft material. To position the natural frequency in the desired range (2 - 3 rad/s), the Smooth-on Ecoflex®Dragon Skin 20 is selected and its Young's modulus is 0.34 MPa. The length of the soft actuator and the number of chambers are couple. The more the number of chambers, the longer the length. The length of 100 mm is chosen to avoid the buckling effect caused by the long structure and the corresponding number of the chamber rooms is 6.

The soft actuator is fabricated by two molds as illustrated in Fig. 2 (b). There are upper and bottom components on the left side of Fig. 2 (b). The Ecoflex®Dragon Skin 20 is in the liquid state, and its curing time is around 4 hours. A flex sensor is embedded into the bottom component as shown Fig. 2 (b) before the liquid rubber becomes a solid state. When the two components are removed from the molds, they are bonded by the silicone adhesive Smooth-on Sil-poxy®, as top right of Fig. 2 (b). The appearance of the soft actuator is demonstrated in bottom right of Fig. 2 (b).

2) *Syringe Pump Design:* The schematic of the syringe pump is shown in Fig. 2 (c), which is used to pressurize soft pneumatic actuators. The design of the syringe pump attempts to reduce the complexity of the pressure control and reduce the weight and size compared to traditional air pumps. The syringe pump, inspired by the hydraulic system, is made of a commercial syringe and a commercial linear

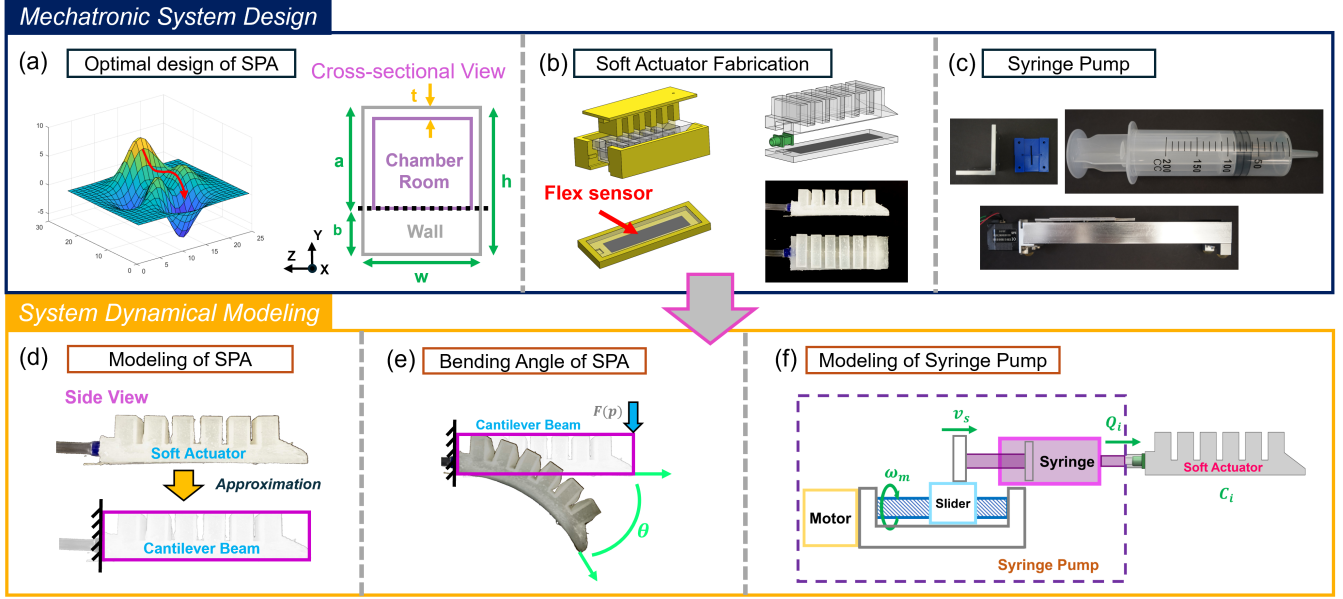


Fig. 2. The design of the mechatronic system can be seen in (a), (b), and (c), while the system modeling is observed in (d), (e), and (f). (a) visualizes how the optimal dimensional parameters are searched in a non-convex space. (b) illustrates the fabrication process of the soft pneumatic actuator and the flex sensor is embedded during the fabrication process. (c) shows the appearance of the syringe pump, and it is made of a commercial linear actuator and a commercial syringe. The (d) and (e) visualize how the structure of the soft actuator is approximated by a cantilever beam and how the bending angle is measured. The modeling schematic of the syringe pump is displayed in (g).

actuator. The syringe pump is driven by the linear motor in the linear actuator [24]. The pressure is adjusted by controlling the position of the slider.

The precision of the linear actuator and the volume of the syringe have an influence on the accuracy and controllability of the syringe pump. The linear actuator, Fulride by NSK Ltd., and a syringe with 150 mL are chosen to fabricate the syringe pump. The accuracy of the Fulride could be μm scale and the volume of the syringe could provide pressurize up to three soft actuators to generate $\pi/2$ rads. Some custom-made components are manufactured by 3D printers in order to assemble the syringe and the linear actuator.

3) *Multi-finger Soft Gripper*: Multiple soft pneumatic actuators and the syringe pump form a soft gripper module, which is assembled by 3D printed connectors and rubber tubes. The detailed compositions of the soft gripper including sensor setup will be described in Sec. IV-C.

B. System Modeling

Prior to designing the algebraic controller for the soft gripper, we need the full system dynamical model of both the soft actuators and the syringe pump. The models of soft actuators and the syringe pump are cascaded to obtain the full system model matrix. The model of each component is built in the following subsection.

1) *Modeling Soft Actuators*: The dynamical model of the soft pneumatic actuator is obtained by modeling its approximated structure as Fig. 2 (d). Due to the large bending nature of the soft actuator, a nonlinear second-order model is utilized

to model and capture its motions. The nonlinear second-order model is described as [28]

$$M_{eq}\ddot{\theta} + C_n\dot{\theta} + K_n\theta^{n+\Delta n} = F(p) \quad (7)$$

where θ is the bending as Fig. 2 (e), $F(p)$ is the equivalent force generated by the input pressure p from the syringe pump, M_{eq} is the equivalent mass of the soft actuator, C_n is the damping constant of the soft actuator. The M_{eq} and C_n currently are estimated by system identification of the true responses in MATLAB, which has an average fitting accuracy of approximately 95.3%. The K_n is the spring constant displayed as

$$K_n = \left(\frac{n+1}{n}\right)^n \left(\frac{EI_n}{L_0^{n+1}}\right) \quad (8)$$

where L_0 is the initial length of the soft actuator, n is the same as the parameter in (6) and it determined by either experiments or data-driven approach [28], I_n is the modified moment of inertia for a large deflection component [25] and it is displayed as

$$I_n = \left(\frac{1}{2}\right)^n \left(\frac{1}{2+n}\right) w(a+b)^{(2+n)} \quad (9)$$

If $n = 1$, the dynamical equations (7), (9), and (8) become linear equations. Given that the linear model is valid from $\theta = 0$ to $4\pi/9$ rads [28], we use $n = 1$ in this research. The (6) is rewritten as

$$\ddot{\theta} + (C_n/M_{eq})\dot{\theta} + (K_n/M_{eq})\theta = c \cdot p/M_{eq} \quad (10)$$

The state-space form is therefore written as

$$A_1 = \begin{bmatrix} 0 & 1 \\ -\frac{K_n}{M_{eq}} & -\frac{C_n}{M_{eq}} \end{bmatrix}, B_2 = \begin{bmatrix} 0 \\ 1 \end{bmatrix}, C_2 = \begin{bmatrix} \frac{c \cdot p}{M_{eq}} \\ 0 \end{bmatrix}^T \quad (11)$$

where $F(P)$ is represented as $c \cdot p$, c is a constant affected by a , b , w , and t [23]. If we stack the system model of n fingers, the state-space form becomes

$$A_{stk} = \begin{bmatrix} A_1 & 0 & 0 \\ 0 & \ddots & 0 \\ 0 & 0 & A_n \end{bmatrix}, B_{stk} = \begin{bmatrix} B_1 \\ \vdots \\ B_n \end{bmatrix}, C_{stk} = \begin{bmatrix} C_1 \\ \vdots \\ C_n \end{bmatrix}^T \quad (12)$$

According to (4), we get the system equation in the Laplace domain. Thus, the system model matrix $P(s)^{n \times 1}$ is described as

$$P(s) = \begin{bmatrix} \frac{c \cdot p/M_{eq_1}}{s^2 + (C_{n_1}/M_{eq_1})s + K_{n_1}/M_{eq_1}} \\ \vdots \\ \frac{c \cdot p/M_{eq_n}}{s^2 + (C_{n_n}/M_{eq_n})s + K_{n_n}/M_{eq_n}} \end{bmatrix} \quad (13)$$

Although the two fingers have the same dimensional parameters such as height, weight, etc., their C_n and K_n in (10) are slightly different due to fabrication errors and uncertainty of soft materials.

$$\begin{aligned} C_1 &\leq C_n \leq C_2 \\ K_1 &\leq K_n \leq K_2 \end{aligned} \quad (14)$$

This nature leads to asynchronized motions when a feedback controller is applied. The asynchronized motions further lead to grasping failure [7]. This study addressed this issue by algebraic control with a single syringe pump and the experimental results will be disclosed in Sec. IV-E.

2) *Modeling Syringe Pump*: The configuration of the syringe pump can be visualized in Fig. 2 (f). The dynamical modeling of the syringe pump starts at the linear motor. When the linear motor works, it will move the slider

$$v_s = \frac{l}{2\pi} \omega_m \quad (15)$$

where v_s is the speed of the motor, l is the lead of the screw inside the linear actuator, and ω_m is the motor speed. The v_s times the inner cross-sectional area of the syringe becomes the output air flow rate

$$Q_i = A v_s = \frac{l}{2\pi} \omega_m \quad (16)$$

where A is the inner cross-sectional area of the syringe, and Q_i is the output air flow rate of the syringe. When Q_i is divided by the capacity of the soft actuator, it becomes the pressure-changing rate inside the soft actuator

$$\dot{p} = \frac{Q_i}{C_i} = \frac{Al}{2\pi C_i} \omega_m \quad (17)$$

The dynamics of the syringe pump is the first-order system. The ω_m has a speed limit of 5 rev/s. The C_i will expand as it is pressurized; however, its effect can be ignored as the input pressure is below 0.1 MPa and the bending angle is below $2\pi/3$ rad. The C_i here is considered as a constant.

The full model of a single soft actuator is the cascade of the (10) and (17).

$$A_1 = \begin{bmatrix} 0 & 1 & 0 \\ 0 & 0 & 1 \\ 0 & -\frac{K_n}{M_{eq}} & -\frac{C_n}{M_{eq}} \end{bmatrix}, B_1 = \begin{bmatrix} 0 \\ 0 \\ 1 \end{bmatrix}, C_1 = \begin{bmatrix} \frac{c \cdot p A l}{2\pi C_i M_{eq}} \\ 0 \\ 0 \end{bmatrix}^T \quad (18)$$

The system is third-order and has a pole at the imaginary axis that makes the system marginally stable. Hence, the full system model matrix $P(s)^{n \times 1}$ in Laplace domain can be obtained by referencing (4) and (12)

$$P(s) = \begin{bmatrix} \frac{c \cdot p A l / 2\pi C_i M_{eq_1}}{s^3 + (C_{n_1}/M_{eq_1})s^2 + (K_{n_1}/M_{eq_1})s} \\ \vdots \\ \frac{c \cdot p A l / 2\pi C_i M_{eq_n}}{s^3 + (C_{n_n}/M_{eq_n})s^2 + (K_{n_n}/M_{eq_n})s} \end{bmatrix} \quad (19)$$

The full system matrix is causal and the minimum phase and the $P(s)$ is full rank and invertible.

C. Controller Design and Analysis

The full system matrix $P(s)$ will be utilized to design the algebraic controller. The system equation can be written as the (5) given the desired $Y(s)_d^{n_u \times 1}$ vector. The system equation is rewritten as

$$\begin{bmatrix} Y_{d1}(s) \\ \vdots \\ Y_{dn}(s) \end{bmatrix} = \begin{bmatrix} P_1(s) \\ \vdots \\ P_n(s) \end{bmatrix} U(s) \quad (20)$$

where $Y_{di}(s)$ represents the desired output of $P_i(s)$, and $1 = 1, \dots, n$. The stable inversion is composed of the feedforward and feedback loop [14]. The feedforward controller is obtained by solving (5) to get $U(s)$ and the additional feedback loop aims to address the system perturbation of the mechatronic system as shown in Fig. 3.

Some theorems are introduced and will be implemented to design the algebraic control including the feedforward control and feedback loop.

Theorem 2. (section III-B, [14]) Let $P(s)$ be non-square ($\text{rank}_{\mathbb{R}(s)}(P) = n_u < n_y$), then there exists an $P^\dagger(s) := (P^*(s)P(s))^{-1}P^*(s)$ satisfying $P^\dagger(s)P(s) = I$. Thus, an approximate solution $U^\alpha(s)$ is defined as

$$U^\alpha(s) = H(s)P^\dagger(s)Y_d(s) \quad (21)$$

satisfying

- 1) $H(s) \in R(s)^{n_u \times 1}$ and is a low-pass filter
- 2) $\|y_d^\alpha(t) - y_d(t)\|_\infty < \infty$ for $t \in [0, \tau]$

- 3) $y_d^a(t) \approx y_d(t)$ for $t \in (\tau, \infty)$
 4) $U^a(s) \in \mathcal{RH}_\infty$ (\mathcal{RH}_∞ represents the Hardy space)

Definition 1. (section III-B, [14]) Let ω_{cl} denote the bandwidth (BW) of the system. So the filter is defined as

$$\begin{aligned} H_i(j\omega) &\approx I \Leftrightarrow \omega \ll \omega_{cl} \\ H_i(j\omega) &\approx 0 \Leftrightarrow \omega \gg \omega_{cl} \\ H_i(j\omega) &\not\approx \{0, I\} \Leftrightarrow \omega \text{ close to } \omega_{cl} \end{aligned}$$

Since the bandwidth of the system is ω_{cl} , the filter is designed by the *Definition 1*. The $H(s)$ of this mechatronic system is designed as a first-order low-pass filter taking the form $\frac{b}{s+a}$, considering its simplicity and stability.

In practice, the system has perturbation or the true system varies with the mathematical system. The system perturbation leads to unexpected dynamics which degrades the performance of the designed controller. Next, we consider the perturbed plant to be a member of all possible plants

$$\Pi \in \{(I + \Delta W_T)P \mid \forall \|\Delta\|_\infty \leq 1\} \quad (22)$$

where the transfer function matrix $W_T \in \mathcal{RH}_\infty$ displays the spatial and frequency characteristics of the uncertainty. The symbol Δ denotes an unknown yet stable function, bounded within a specific norm [29]. A general approach to defining the robustness weight function W_T is described below [30].

$$\left| \frac{M_{ik}e^{j\phi_{ik}}}{M_i e^{j\phi_i}} - 1 \right| \leq |W_T(j\omega_i)|, i = 1, \dots, m; k = 1, \dots, o \quad (23)$$

The magnitude and phase values are assessed over a range of frequencies, denoted as ω_i (ranging from $i = 1$ to m), and the experiment is repeated $n = 5$ times. The notation (M_{ik}, ϕ_{ik}) refers to the magnitude-phase measurements corresponding to frequency ω_i and the k th experiment iteration. Similarly, (M_i, ϕ_i) represents the magnitude-phase pairs for the nominal plant T .

The error system (with perturbed term) can be compensated by using the output feedback as displayed in Fig. 3. The u_{ff} is calculated based on the *Theorem 2*. It is assumed that the output of the real (uncertain) system can be measured such as sensors or observers. Since the nominal system output can be computed with the combined input u_c , we have the output difference $y_\Delta(t)$. With this output difference, we can compensate for the error by the following theorem.

Theorem 3. [14] Consider the block diagram in Fig. 3 with (22). Then the bounded U_{fb} yields $\|y_d(t) - \tilde{y}(t)\|_\infty \rightarrow 0$ iff $\tilde{Y}(s) \in \text{Im}_{\mathbb{R}(s)}(P)$.

For simplicity, we take ΔW_T as Δ , and consider $\tilde{P}(s) \in \Pi$, $Y_d = P U_{ff}$, and $U_c(s) := U_{ff} - U_{fb}$ (by referencing Fig. 3)

$$\tilde{P}(s)U_c(s) = \tilde{Y}(s) = P U_c + \Delta_u P U_c \quad (24)$$

$$P U_{ff} + \Delta_u P U_{ff} - P U_{fb} - \Delta_u P U_{fb} = \tilde{Y}(s) \quad (25)$$

$$\Rightarrow P U_{fb} = \Delta_u P U_{ff} - \Delta_u P U_{fb} \quad (26)$$

The feedback loop will compensate for the model errors. The detail proof of *Theorem 2* and *3* can be referenced in [14].

The model inversion and feedback loop are introduced to achieve accurate tracking of the system. The next problem is

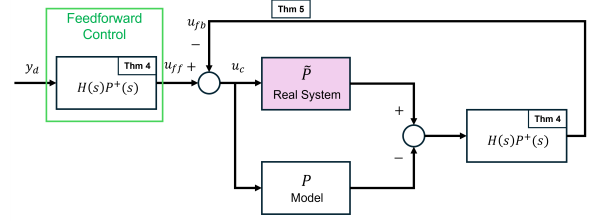


Fig. 3. The block diagram of the algebraic controller including the feedforward control and feedback loop.

whether the system performance can be achieved by underactuated control as depicted in (5). That is, we control multiple soft actuators with a single input pressure. Here, we intend to synchronize the motions of the multi-finger gripper to reach stable grasping [7]. The desired response of each finger is set as the same so the (20) becomes

$$\begin{bmatrix} Y_d(s) \\ \vdots \\ Y_d(s) \end{bmatrix} = \begin{bmatrix} P_1(s) \\ \vdots \\ P_n(s) \end{bmatrix} U(s) \quad (27)$$

$$\Rightarrow Y_d(s) = P(s)U(s) \quad (28)$$

where $Y_d(s) \in \text{Im}_{\mathbb{R}(s)}(P)$. We are going to show that this problem is solvable and the solution exists by mathematics inference. Since the $P(s)$ has full rank = 1, the $P(s)$ is invertible and exists left inverse matrix according to the *Theorem 2*. The inverse matrix is $P^\dagger(s) = (P^*(s)P(s))^{-1}P^*(s)$. The controller is obtained by $U(s) = H(s)P^\dagger(s)Y_d(s)$. Therefore, there exists input $U(s)$ that makes the $Y_d(s)$ achievable.

Furthermore, if the system is controllable, the controllability matrix of the (5) is defined as $M_c = [A \ BA \ BA^2 \ \dots]$. The set $\mathbb{S}_n \subset \mathbb{R}$ is assumed as the *synchronization subspace* [31]. Now we define the controllability of the (28).

Definition 2. The system matrix $P(s)$ in (28) is minimal and controllable if $\mathbb{S}_n \subset M_c$.

The single input may fail to synchronize the motions of soft fingers with the same dimensional parameters because of the uncertainty of the soft materials. The deformation curves of soft materials exhibit high uncertainty when they have a slow deformation rate [20]. In contrast, the curves demonstrate much less uncertainty when their deformation rate is high. Similarly, when the higher pressure changing rate is applied to soft fingers, they show less uncertainty, align with nominal behaviors, and tend to have synchronized motions. This property influences the controllability of the synchronization of the multi-finger soft gripper (28) and the existence of the subspace \mathbb{S}_n .

IV. EXPERIMENTAL EVALUATION

In previous sections, we introduce the mechatronic system, specifically the multi-finger soft gripper, alongside system dynamical models and control algorithms. Prior to experimentation, preliminary tests are conducted using analytical

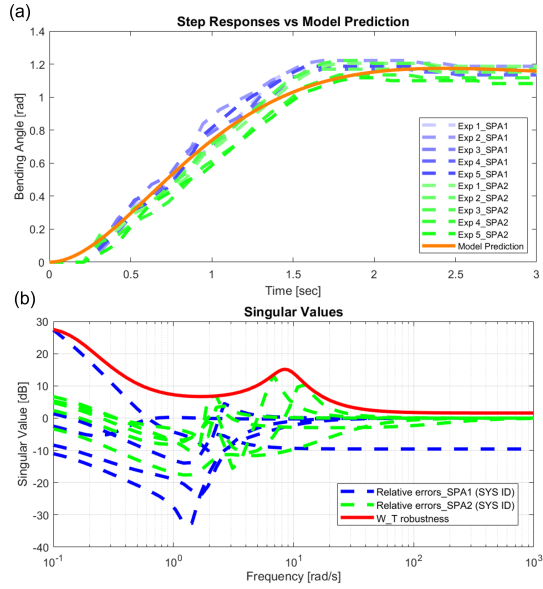


Fig. 4. Several open-loop responses of both soft pneumatic actuators (soft fingers) are demonstrated in (a). The robustness weight selection based on the modeling errors can be seen in (b).

software to assess the feasibility of the algebraic controller. Subsequently, a series of experiments are executed to evaluate the practicality of the proposed control approach. Additional disturbance tests are then performed to evaluate the robustness of the controller.

A. Preliminary Evaluations

Some definitions and assumptions are applied in Sec. II and III, so this subsection intends to evaluate that the definitions and assumptions are valid before the simulations and experimentation.

1) *Model Evaluation*: The analytical model matrix is built for the mechatronic system as the $P(s)$ in (29). Based on the discussion in Sec. III-C, the model has uncertainty and will cause modeling errors due to the uncertain soft materials. The bounded model uncertainty is assumed, $\|\Delta\|_{\infty} \leq 1$ in (22). Several step responses of both soft fingers are conducted to evaluate whether the model uncertainty is bounded.

Figure 4 (a) demonstrates the repeated step responses of both soft actuators, the first (blue) and second (green) element of the $P(s)$ in (29). The system performance varies due to the properties of soft materials [7]. The singular value of the bounded constraint can be found in Fig. 4 (b). The system perturbation of two soft actuators is bounded. Specifically, it is observed that $\|C_n - C_{nominal}\| \leq 14.3\%$ and $\|K_n - K_{nominal}\| \leq 5.9\%$ by system identification of the step responses in Fig. 4 (a). Two soft actuators, both elements of the $P(s)$ in (29), show a similar result. We can conclude that the perturbations of the two systems are bounded.

2) *Controllability Evaluations*: Another preliminary evaluation is needed before the experimentation. The system equation of (4) should be controllable and observable. The controllability matrix $M_c = [A \ BA \ BA^2 \ \dots]$ and the

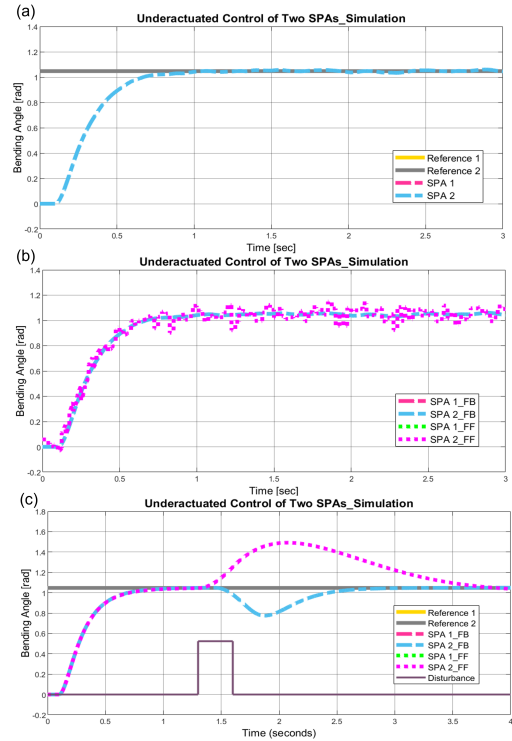


Fig. 5. The simulation results of the two-finger gripper are shown in (a). The sensor noise and disturbance are considered and displayed in (b) and (c).

observability matrix $M_o = [C \ CA \ CA^2 \ \dots]^T$ of (4) both have full rank, so the full system is controllable and observable. Since the full system is controllable and observable, the system realization is also minimal. This evaluation matches the *Assumption 1*. The designed algebraic controller is valid.

B. Simulation Results

Section II-B introduces the general case of the problem (5). The system matrix $P(s)$ comprises n elements. Simulations will be conducted on multi-finger soft gripper systems to assess different scenarios, with n taking values of 2 and 3 for $P(s)$, respectively. The simulations help us understand if the controller can work and make adjustments. For example, the low pass filter $H(s)$ of *Theorem 4* will be adjusted to achieve better tracking performance.

1) *Two-finger Gripper Simulation*: The first simulation is performed on a two-finger gripper, which includes two soft actuators (soft fingers) and a single syringe pump. The desired output is selected as a step response $\frac{\pi/3}{s} \in \text{Im}_{\mathbb{R}(s)}(P)$ considering the applications. The desired output ($\pi/3$) may lead to the collision of the two soft fingers as Fig. 1, but we aim to check the performance of the control algorithm. The system equation is written as

$$\begin{bmatrix} \frac{\pi/3}{s} \\ \frac{\pi/3}{s} \end{bmatrix} = \begin{bmatrix} \frac{7.831}{s^3 + 2.66s^2 + 3.61s} \\ \frac{7.831}{s^3 + 2.45s^2 + 3.06s} \end{bmatrix} U(s) \quad (29)$$

The controller is obtained based on the *Theorem 2* and 3, so the $H(s)$ is designed as $5/s$ and $P^\dagger(s) = \left[\frac{s^3 + 2.66s^2 + 3.61s}{15.66}, \frac{s^3 + 2.45s^2 + 3.06s}{15.66} \right]$.

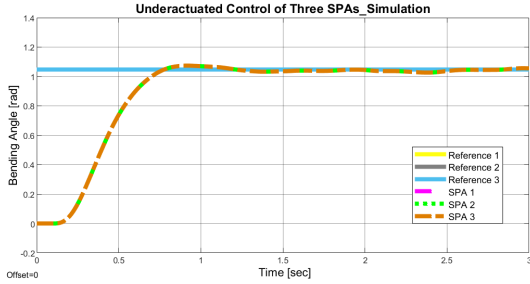


Fig. 6. The simulation result of the three-finger soft gripper is demonstrated. Their models are different but their motions are synchronized by the algebraic controller.

This controller is able to synchronize the motions of the two fingers within the soft gripper as in Fig. 5 (a). The settling time of both fingers is below 1 *sec*. To further evaluate the performance of the controller, sensor noise and disturbance are added as Fig. 5 (b) and (c). The feedback loop can compensate for the sensor noise as Fig. 5 (b). The root-mean-square error (RMSE) of the sensor noise is around ± 2 *deg* [7]. The RMSE of the feedforward control only and feedforward and feedback control of simulations are approximately 5 *deg* and 2.3 *deg* respectively. Thus, the feedback loop outperforms in handling the noise.

The disturbance here is regarded as the soft fingers are hitting by an external force. The results show that the controller is capable of adjusting the system back to the reference faster than feedforward control as Fig. 5 (c). Moreover, the amplitude of the errors of feedforward controller (0.4 *rad*) is larger than that of the feedback loop (0.2 *rad*). The simulation results validate the *Theorem 3* and (26). The experimental results can be referenced in Sec. IV-E and IV-F.

2) *Three-finger Gripper Simulation*: The algebraic controller displays the desired performance in the two-finger gripper simulations. Next, the simulation is extended to a three-finger gripper. The reference is the same and it is $\frac{\pi/3}{s} \in \text{Im}_{\mathbb{R}(s)}(P)$. This desired output will also lead to collision of the three fingers but the simulation here aims to evaluate the performance of the controller.

$$\begin{bmatrix} \frac{\pi/3}{s} \\ \frac{\pi/3}{s} \\ \frac{\pi/3}{s} \end{bmatrix} = \begin{bmatrix} \frac{7.831}{s^3+2.66s^2+3.61s} \\ \frac{7.831}{s^3+2.76s^2+3.88s} \\ \frac{7.831}{s^3+2.45s^2+3.06s} \end{bmatrix} U(s) \quad (30)$$

The $H(s)$ is designed as $5/s$ and $P^\dagger(s) = \left[\frac{s^3+2.66s^2+3.61s}{23.49}, \frac{s^3+2.76s^2+3.88s}{23.49}, \frac{s^3+2.45s^2+3.06s}{23.49} \right]$.

The simulation results are demonstrated in Fig. 6. The controller is able to synchronize the three-finger soft gripper and the motions of the three fingers are aligned. Their response time is all below 1 *sec*.

3) *Summary*: The simulation results on two-finger and three-finger soft grippers endorse the feasibility of the algebraic controller. The motions of fingers are synchronized in both the transient and steady states. The synchronization will enable the grasping success rate when the soft gripper is applied to manipulate various objects. The controller will be

applied to the real soft gripper to evaluate the applicability of the algebraic control algorithms.

C. Experimental Setup

Figure 1 illustrates both the experimental arrangement and the signal flow diagram. The two-finger soft gripper is used to conduct the experiments with a single syringe pump. The soft actuators are fabricated by molds as illustrated in Fig. 2 (b). The motions of the soft fingers are driven by the syringe pump [24], which is actuated by a stepper motor. An air pressure sensor (Walfront, Lewes, DE) with a sensing range of 0 to 80 *psi* is utilized to detect the air pressure for open-loop control. Additionally, each soft finger contains a flex sensor (Walfront, Lewes, DE) inside to monitor its bending angle, facilitating feedback control. The flex sensor is a resistive type sensor and has a sensing range of 100 *deg* and sensing error is approximately 2 *deg* (root-mean-square error). Both sensors are synchronized with Arduino MEGA 2560 (SparkFun Electronics, Niwot, CO), which is based on the Microchip ATmega 2560. The controller algorithms are programmed in MATLAB/Simulink which is communicated with the Arduino MEGA 2560 to process feedback signals and generate control commands for the mechatronic system. The model and controller are discretized in the analytical software with a sampling time of 100 *ms*. The "Real System" block in Fig. 3 is replaced by the real soft gripper.

D. Open-loop & Closed-loop Tests

Prior to implementing the algebraic controller, the open-loop tests attempt to visualize the open-loop responses of the soft fingers. The soft fingers have the same dimensional parameters such as height, width, length, etc. Nonetheless, their system parameters of (19) are different which leads to asynchronized motions. In applications, the open-loop control results in grasping failure of the soft gripper [7] due to the asynchronized motions of its fingers. The open-loop test results are illustrated in Fig. 7 (a).

The blue dashed line represents the response of the left finger (SPA 1) in Fig. 1 while the green dashed line denotes the right finger (SPA 2) in Fig. 1. The left finger is active and responds faster. By contrast, the right finger has relatively slow responses. Their steady states are also different due to different system parameters of (19). The left finger reaches approximately 47 *deg* while the right finger reaches around 40 *deg* with a reference 45 *deg*.

Moreover, the closed-loop test is performed by using a single LQR controller for two soft fingers. The accuracy and response time of both fingers are improved; however, their motions are not synchronized in Fig. 7 (a). The right finger has a steady-state error of around 4–5 *deg* compared to the reference. Thus, a single LQR is unable to synchronize the motions of two fingers due to their model variations.

E. Stable Inversion Control Tests

The stable inversion controller designed in Sec. III-C is implemented to control and synchronize the two fingers in

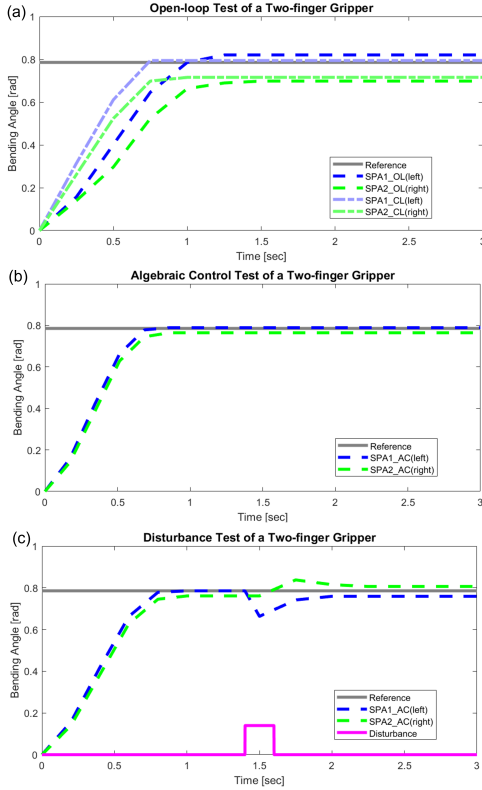


Fig. 7. The visualization of the open-loop test and LQR control of the two-finger gripper is asynchronous as displayed in (a). The algebraic control result is demonstrated in (b). The motions of the two fingers are synchronized compared to the results in (a). The disturbance test is disclosed in (c) and the controller can handle the external disturbance.

this subsection. The result is demonstrated in Fig. 7 (b). The motion of two soft fingers is synchronized and they reach a steady state at nearly the same time with nearly no errors. Compared to open-loop and LQR control, the controller enables more precise and synchronized motions for both soft fingers with a single syringe pump. Their motions are synchronized with around 2 deg differences. Our previous work [7] utilized a syringe pump for each soft finger of the two-finger gripper to reach synchronization. However, one more syringe pump is needed compared to this research. If there are three-finger or four-finger grippers, more syringe pumps are required, which implies more costs, space, and weight. That makes the applications of the soft gripper setup more difficult.

F. Disturbance Tests

According to the *Theorem 3*, the feedback loop is designed to deal with the model errors or disturbances caused by external forces. The disturbance is given at around $t = 1.4$ sec when the fingers arrive at the steady state as Fig. 7 (c). The external force is only applied to the left finger. The algebraic controller is able to adjust the systems to the desired reference when the external force is applied. The experimental results support the *Theorem 3*.

V. DISCUSSION AND CONCLUSION

A. Discussion

The proposed control algorithms successfully synchronize the motions of two soft fingers within a soft gripper. The performance is validated by the real-world experimentation. However, there is a limitation of using this control algorithm in which the desired output function of (28) should be in the image space of the model matrix $P(s)$. If the desired output function is out of the image space of $P(s)$, the proposed method is no longer valid. For instance, if the desired function of one finger is $\pi/4$ and another one is $-\pi/4$, the solution of (28) does not exist. The negative bending angle is out of the image space of this soft gripper. Specifically, since the desired functions are in the image space of the model matrix, the position and its derivative are constrained by the output functions. Unlike the linear quadratic regulator, the position and velocity can be adjusted by selecting a suitable weighting matrix function. In short, the synchronization of the desired systems is achievable but the output function cannot be randomly selected.

The existence of the *synchronization subspace* is discussed in Sec. III-C. The results of the Sec. IV-E and Fig. 7 (b) support the discussion and *Definition 2*. The open-loop control has a slower input command and the responses of both fingers differ as Fig. 7 (a). The stable inversion control has a faster input command and the motions of the two soft fingers are synchronized as Fig. 7 (b). It, therefore, can be concluded that the (28) is controllable and the *synchronization subspace* exists. Note that the LQR control also has faster responses but its command trajectory is different from that of stable inversion control. The result of LQR control displays that it does not belong to the *synchronization subspace*.

B. Conclusion

This paper explores the underactuated control of multiple fingers within a soft gripper, validating a controller that contain feedforward and feedback loops designed via algebraic methods. The soft fingers are designed based on an optimal design framework and their dynamical models are obtained by applying nonlinear mechanics. The feedforward controller is designed based on stable inversion of the system model matrix, while the feedback loop is incorporated to handle the system perturbations. Simulation results demonstrate the efficacy of the control algorithms in synchronizing both two-finger and three-finger grippers. Experimental validation further confirms the feasibility of synchronizing motions within a two-finger gripper setup. Even if there is a disturbance, the controller is able to adjust the systems to the reference. The control strategy reduces the number of inputs (air pumps) which may benefit the implementation of multi-finger soft grippers.

In the future, the proposed control theories will be extended to broader cases. The desired output functions are now restricted to the range space of the system model. The extended research will discuss if any solution exists when the desired output functions are out of the image space of the system model theoretically and experimentally.

ACKNOWLEDGMENTS

The authors would like to thank NSK, Ltd. for arranging the linear actuators used in the experiments.

REFERENCES

- [1] E. Navas, R. Fernández, D. Sepúlveda, M. Armada, and P. Gonzalez-de Santos, "Soft grippers for automatic crop harvesting: A review," *Sensors*, vol. 21, no. 8, p. 2689, 2021.
- [2] T. George Thuruthel, Y. Ansari, E. Falotico, and C. Laschi, "Control strategies for soft robotic manipulators: A survey," *Robotics and Autonomous Systems*, vol. 125, p. 103427, 2020.
- [3] F. Iida and C. Laschi, "Soft robotics: Challenges and perspectives," *Procedia Computer Science*, vol. 7, no. 1, pp. 99–102, 2011.
- [4] W.-T. Yang and M. Tomizuka, "Design a multifunctional soft tactile sensor enhanced by machine learning approaches," *ASME Journal of Dynamic Systems, Measurement, and Control*, vol. 144, no. 8, p. 081006, 2022.
- [5] G. Alici, T. Canty, R. Mutlu, W. Hu, and V. Sencadas, "Modeling and experimental evaluation of bending behavior of soft pneumatic actuators made of discrete actuation chambers," *Soft Robotics*, vol. 5, no. 1, pp. 24–35, 2018.
- [6] K. G. Demir, Z. Zhang, J. Yang, and G. X. Gu, "Computational and experimental design exploration of 3d-printed soft pneumatic actuators," *Advanced Intelligent Systems*, vol. 2, p. 7, 2020.
- [7] W.-T. Yang, B. Kurkcu, M. Hirao, L. Sun, X. Zhu, Z. Zhang, G. X. Gu, and M. Tomizuka, "Control of soft pneumatic actuators with approximated dynamical modeling," in *IEEE International Conference on Robotics and Biomimetics (ROBIO)*. IEEE, 2023, pp. 1–8.
- [8] J. Zhou, J. Huang, X. Ma, A. Lee, K. Ksougé, and L. Y.-H. Liu, "Design, modeling, and control of soft syringes enabling two pumping modes for pneumatic robot applications," *IEEE/ASME Transactions on Mechatronics*, 2024.
- [9] E. H. Skorina, M. Luo, S. Ozel, F. Chen, W. Tao, and C. D. Onal, "Feedforward augmented sliding mode motion control of antagonistic soft pneumatic actuators," in *2015 IEEE International Conference on Robotics and Automation (ICRA)*. IEEE, 2015, pp. 2544–2549.
- [10] E. H. Skorina, W. Tao, F. Chen, M. Luo, and C. D. Onal, "Motion control of a soft-actuated modular manipulator," in *2016 IEEE International Conference on Robotics and Automation (ICRA)*. IEEE, 2016, pp. 4997–5002.
- [16] P. Pustina, C. D. S. Santina, and A. D. Luca, "Feedback regulation of elastically decoupled underactuated soft robots," *IEEE Robotics and Automation Magazine*, vol. 7, no. 2, pp. 4512–4519, 2022.
- [17] J. Forney and G. David, "Minimal bases of rational vector spaces, with applications to multivariable linear systems," *SIAM Journal on Control*, vol. 13, no. 3, pp. 493–520, 1975.
- [18] D. S. Dummit and R. M. Foote, *Abstract algebra*. Springer Science and Business Media, 2004, vol. 3.
- [19] E. N. Antoniou, A. I. G. Vardoulakis, and S. Vologiannidis, "Numerical computation of minimal polynomial bases: A generalized resultant approach," *Linear algebra and its applications*, vol. 405, pp. 264–278, 2005.
- [20] J. C. Case, E. L. White, and R. K. Kramer, "Soft material characterization for robotic applications," *Soft Robotics*, vol. 2, no. 2, pp. 80–87, 2015.
- [11] E. H. Skorina, M. Luo, W. Tao, F. Chen, J. Fu, and C. D. Onal, "Adapting to flexibility: model reference adaptive control of soft bending actuators," *IEEE Robotics and Automation Letters*, vol. 2, no. 2, pp. 964–970, 2017.
- [12] Z. Q. Tang, H. L. Heung, K. Y. Tong, and Z. Li, "Model-based online learning and adaptive control for a "human-wearable soft robot" integrated system," *The International Journal of Robotics Research*, vol. 40, no. 1, pp. 256–276, 2021.
- [13] C. M. Best, M. T. Gillespie, P. Hyatt, L. Rupert, V. Sherrod, and M. D. Killpack, "A new soft robot control method: Using model predictive control for a pneumatically actuated humanoid," *IEEE Robotics and Automation Magazine*, vol. 23, no. 3, pp. 75–84, 2016.
- [14] B. Kurkcu and M. Tomizuka, "Algebraic control: Complete stable inversion with necessary and sufficient conditions," *IEEE Transactions on Automatic Control*, 2024 (Under revision).
- [15] M. Keppler, C. O. Ott, and A. Albu-Schäffer, "From underactuation to quasi-full actuation: Aiming at a unifying control framework for articulated soft robots," *International Journal of Robust and Nonlinear Control*, vol. 32, no. 9, pp. 5453–5484, 2022.
- [21] W.-T. Yang, B. Kurkcu, and M. Tomizuka, "Optimized design of a soft actuator considering force/torque, bendability, and controllability via an approximated structure," *ASME Journal of Mechanical Design*, 2024.
- [22] G. F. Franklin, J. D. Powell, A. Emami-Naeini, and J. D. Powell, *Feedback control of dynamic systems*. Upper Saddle River: Prentice hall, 2002, vol. 4.
- [23] W.-T. Yang, H. S. Stuart, and M. Tomizuka, "Mechanical modeling and optimal model-based design of a soft pneumatic actuator," in *IEEE International Conference on Soft Robotics (RoboSoft)*. IEEE, 2023, pp. 1–7.
- [24] W.-T. Yang, M. Hirao, and M. Tomizuka, "Design, modeling, and parametric analysis of a syringe pump for soft pneumatic actuators," in *IEEE/ASME International Conference on Advanced Intelligent Mechatronics (AIM)*. IEEE, 2023, pp. 317–322.
- [25] K. Lee, "Large deflections of cantilever beams of non-linear elastic material under a combined loading," *International Journal of Non-Linear Mechanics*, vol. 37, no. 3, pp. 439–443, 2002.
- [26] Z. Wang and S. Hirai, "Chamber dimension optimization of a bellows-type soft actuator for food material handling," in *IEEE International Conference on Soft Robotics (RoboSoft)*. IEEE, 2018, pp. 382–387.
- [27] J. Wang, Y. Fei, and W. Pang, "Design, modeling, and testing of a soft pneumatic glove with segmented pneumatic bending actuators," *IEEE/ASME Transactions on Mechatronics*, vol. 24, no. 3, pp. 990–1001, 2019.
- [28] W.-T. Yang, H. S. Stuart, B. Kurkcu, and M. Tomizuka, "Nonlinear modeling for soft pneumatic actuators via data-driven parameter estimation," in *IEEE/ASME International Conference on Advanced Intelligent Mechatronics (AIM)*. IEEE, 2024.
- [29] K. Zhou and J. C. Doyle, *Essentials of robust control*. Upper Saddle River, NJ: Prentice hall, 1998, vol. 104.
- [30] J. C. Doyle, B. A. Francis, and A. R. Tannenbaum, *Feedback control theory*. Courier Corporation, 2013.
- [31] S. E. Tuna, "Synchronization of linear systems via relative actuation," *Systems and Control Letters*, vol. 134, p. 104527, 2019.